Scripta Materialia 182 (2020) 114–119

Contents lists available at ScienceDirect

Scripta Materialia

journal homepage: www.elsevier.com/locate/scriptamat

Understanding mechanical behavior of metallic foam with hollow struts using the hollow pentagonal dodecahedron model

Rui Dai[a], Meng Wang[b], Dini Wang[c], Zengrong Hu[d], Matthew D. Green[b], Qiong Nian[a,c,*]

[a] Department of Mechanical Engineering, School of Engineering for Matter, Transport and Energy, Arizona State University, Tempe, AZ 85281, United States
[b] Department of Chemical Engineering, School of Engineering for Matter, Transport and Energy, Arizona State University, Tempe, AZ 85281, United States
[c] Department of Material Science and Engineering, School of Engineering for Matter, Transport and Energy, Arizona State University, Tempe, AZ 85281, United States
[d] School of Rail Transportation, Soochow University, Suzhou, Jiangsu, 215131, China

ARTICLE INFO

Article history:
Received 8 January 2020
Revised 1 March 2020
Accepted 2 March 2020

Keywords:
Cellular material
Metallic foam
Hollow strut
Pentagonal dodecahedron
Elastic modulus

ABSTRACT

Nickel (Ni) foam with hollow struts, as one type of ultralight stochastic cellular material, can be simply manufactured by electroplating on a thermally or chemically removable template. A fundamental understanding is required to create a consistent lattice model with capability to capture its mechanical behavior. Herein, an unprecedented hollow pentagonal dodecahedron (HPD) model is proposed with a novel 3D packing architecture. HPD model reveals the scaling of Young's modulus (E) to relative density (ρ') in the factor of 2, which agrees well with uniaxial compression tests. This simplified model paves a way to investigate the cellular material with hollow struts.

Mechanical metamaterials, either periodically or stochastically architected from nanoscale to microscale, are able to combine structure and host material together and thus enable a wide range of material properties not commonly found in nature [1]. Cellular metallic material is one such subset, which attracts enormous attention in applications ranging from structure supporting frames to passive heat dissipation, battery electrodes, automotive, railway, and etc. [2]. The increased interests in cellular metallic materials is attribute to their exceptional characteristics including high strength-to-weight ratio, light weight, super large surface area combining with excellent thermal and electrical properties [3].

These cellular metallic materials can be manufactured through precision casting [4], powder metallurgy [5], injection molding [6,7], polymer templated deposition [8], or additive manufacturing [9], and can either be closed or open cell, stochastic, or periodic in architecture [10]. It is noteworthy that in recent years the versatility of manufacturing for various metal alloys (Ni-P, Ni-Cu, Ni-W-P) [11] with electroless-electroplating and additive manufacturing for polymer templates [12] engenders unbound potential design space by which new cellular metallic material can be created, including both stochastic and topology-optimized architectures. For instance, Queheillalt et al. [13] manufactured stochastic open cell metal foam through polymer templated physical vapor deposition. The deposition process is based on an open-cell polymer foam template, e.g., polyurethane (PU) foam, upon which a conformal metal alloy layer is deposited onto the surface of the struts. Using a similar strategy, but with cost-effective electroless-electroplating method, Schaedler et al. [11] created a novel periodical Nickel (Ni) based micro-lattice with structural hierarchy spanning from nanometers to millimeters. The author showed that the architected structure can achieve efficient material utilization, with the Young's modulus scaling as $E \sim \rho^2$, and was able to recover from more than 50% compression deformation at ultralight densities (relative densities of $< 0.1\%$), which demonstrates large kinetic energy absorption ability upon cyclic loading. Additionally, this electroless-electroplating method has been utilized to manufacture stochastic Ni foam by Jung et al. [14], during which the authors concluded that the polymer template core only had a marginal effect on the mechanical properties and hence can be neglected for performance analysis.

Despite a number of studies have been conducted, there are still challenges related to the structural interpretation of those cellular metallic materials, especially with hollow struts. For example, few studies delve into the stochastic architecture enhancement of metal alloy structure on the polymer template, how the metal alloy enhancement occurs, and to what extend the enhancement could be. And, few guiding principles exist for designing the

* Corresponding author.
E-mail address: qiong.nian@asu.edu (Q. Nian).

https://doi.org/10.1016/j.scriptamat.2020.03.001
1359-6462/

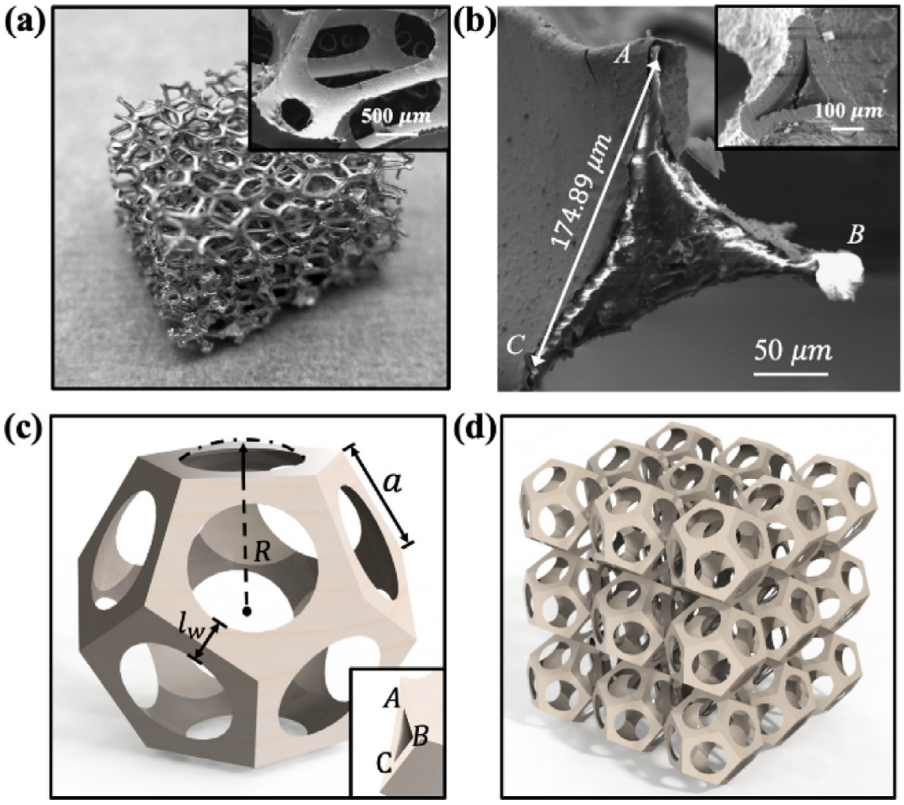

Fig. 1. **(a)** Optical image of the open-cell Ni foam, insert is the architecture of the copper coated PU foam as the template. **(b)** Representative SEM image of a single strut in copper coated PU foam template, insert is the hollow Ni strut after template removal. **(c)** A unit cell of HPD model and its lattice parameters. **(d)** 3D packing of the HPD unit cells.

foam-like architecture that efficiently integrates the structure and microstructural deformation mechanisms [4,10]. Most previous studies concentrate on the modeling of cellular metallic materials, but with solid struts, such as Kelvin structures [15] and Weaire-Phelan structures [16], both of which were developed on the idea of the surface area minimization. Kwon et al. [17], developed a Tetrakaidecahedral frame structure as a representative unit-cell that can predict the stiffness of metallic foam agreeing well with experimental data. X-ray computed tomography is also used for cellular solids modeling, though prior studies reported that the prediction leads to a systematic overestimation of the elastic properties [18]. To the authors' knowledge, an architected model that can describe the elastic behavior of cellular metallic material with hollow struts remains rare. In addition, unlike topology optimized structures, stochastic structures bring extra challenges due to not only the uncertainty combination of their underline lattice but also the reticulation and the redundancy of these combinations. Nevertheless, understanding the complex interplay between the topology of the hollow strut foam structure and the constituent materials is crucial for optimizing and designing complex topological structures with tunable mechanical properties.

In this work, an unprecedented hollow pentagonal dodecahedron (HPD) lattice model is developed to study the mechanical behavior of the stochastic metallic foam with hollow struts, which is manufactured by PU foam templating and Ni electroless-electroplating as shown in Fig. 1(a). This templated Ni foam normally possesses a uniform three-dimensional reticulated structure that is comprised of various unit cells with different size and shape suggesting an isotropic architecture. Fig. 1(b) shows the geometrical size and shape of a single strut (insert shows the hollow Ni strut, more details seen in supporting materials). To mimic the architecture of this as-manufactured stochastic foam, a pentagonal dodecahedron (PD) model following prior studies [19–21] has been developed, but with an innovative strategy to create hollow struts for the first time (more details seen in supporting materials) in Fig. 1(c). This HPD unit cell is chosen as a representative volume elementary (RVE), while a novel 3D packing architecture for HPD lattices is proposed to enable a potential periodic boundary condition (PBC) as shown in Fig. 1(d). Then, Finite Element Method (FEM) simulations are applied on the as-built monolithic unit cell with Ni as the constituent material to assess its capability of interpreting the mechanical behavior of Ni foam with hollow struts. The simulation results are validated by comparing to both the experimental compression tests and the theoretical power coefficient law drawn from an analytical model considering the bending, stretching and shearing behavior of representative strut as Timoshenko beam subject to the uniaxial compression stress. Moreover, the stress distribution on struts are studied to understand the potential mechanical failure (fracture) of the HPD lattice architecture.

Fig. 2 shows the compression behavior of an HPD unit cell in the wall thickness of 25 μm. Stress contours of 0.2%, 1%, 2% and 3% volume averaged strain are shown in Fig. 2(a) – (d). At a small strain of 0.2%, it is clear to observe the stress concentration in the HPD lattice starts to appear near the end of the struts, implying the collapse of the struts always tend to occur near the clamped area. This is corresponding to the theory that plastic deformation always originates near or at the "node" region [22]. As the deformation continues to larger strain, plastic deformation will propagate through the whole struts indicating the whole structure reaches the plastic deformation stage and the struts may start to collapse by the plastic localization (i.e. buckling and necking)[23,24]. Besides, the uneven stress distribution across different struts implies they will not fail at the same time leading to the consecutive failure of the lattice structure. This phenomenon has been demon-

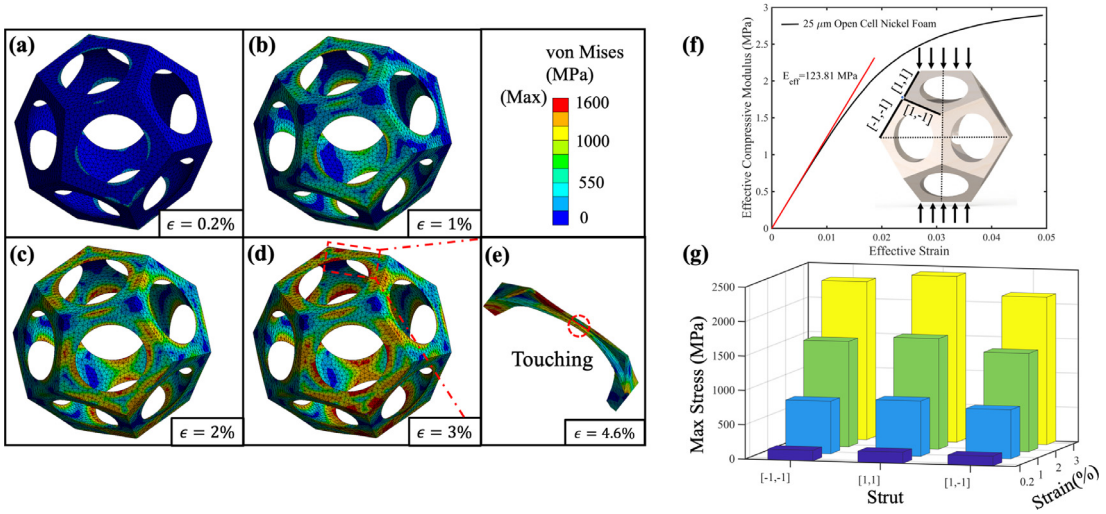

Fig. 2. **(a)-(d)** The stress contour of the HPD unit cell deformed under a series of volume averaged strains; **(e)** a cross-section view of the inner surface of a hollow strut deformed under 5.3% volume averaged strain; **(f)** engineering stress-strain curve of the HPD unit cell with wall thickness of 25 μm, note: the modulus is derived from the first 0.2% effective strain assumed to be linear. The inset image shows the struts of the HPD unit are classified to three different types; **(g)** Statistical analysis showing the maximum equivalent stress on the outer surface around the center of the three different types of struts.

strated by prior experiments as well. For example, Torrent et al. [10] showed that the failures on the strut structure were a main reason leading to the decrease of the mechanical strength of cellular metallic material. Whereas, for this hollow structure, the outer surface generally exhibits larger deformation than the inner surface. As a result, the breaks will occur on the outer surface first followed by the inner surface; therefore, there won't be a steep stress drop during compression, which contrasts with solid counterpart materials. As the deformation continues to around 4.6% volume averaged strain as shown in Fig. 2(e), the inner surface and the outer surface will be in contact with each other resulting in a reinforcement on the strength of the beam. These results demonstrate that a superior mechanical property could be achieved by applying a hollow strut structure compared to a solid strut, especially at the same relative density level, which agrees well with Queheillalt's results [13].

To interpret which strut initiates the mechanical failure in our HPD architecture, we classified all the struts into three types with respect to their position considering the symmetry and ignoring the PBC boundary struts, as shown in Fig. 2(f). For a quick reference, these struts are labeled as [1,1], [−1,1] and [1,−1]. The sign and the number are not the Cartesian coordination while only implying their rough position. The maximum stress on the surface of each strut is extracted based on different strain levels shown in Fig. 2(g). The [−1, −1] strut normally possesses largest stress level among all strut. From above, it can be concluded [−1, −1] strut is the start position for the peak stress to reach and the stress on the plane orthogonal to [−1,1] direction contributes to the formation of a shear band and eventually a macroscale slip bands evolved. This phenomenon is also observed by E. Amsterdam [23]. Note this, for the bending dominated HPD lattice, bending rigidity generated with the compression of the inner surface and tension of the outer one, makes it feasible to only consider the stress distribution on the outer surface of the struts.

In order to derive the effective modulus of the Ni foam with hollow struts, the stress-strain relationship of the HPD lattice architecture in the wall thickness of 25 μm is plotted in Fig. 2(f). Typically, for a cellular metallic structure with the elastic deformation strain less than 0.2%, the plot tends to be in linear shape. The slope of the linear curve could be extracted to reflect the effective modulus of the material. Applying this strategy, the slope of the linear curve in Fig. 2(f) is extracted to be 123 MPa, which is comparable to the normalized result of Torrent's study [10]. Note that the deviation of the modulus results of HPD with prior studies of Ni micro-lattice is owing to the topology difference between them. For example, the octet-truss lattice architecture in Torrent's study has node connectivity of 12, however, the node connectivity is 6 for the 3D packing HPD lattice architecture, suggesting a weaker mechanical response.

The z direction compressive stress-strain response for five represented HPD unit cells we considered with wall thickness from 10 μm to 50 μm is shown in Fig. 3. The maximum stress value on the struts, at elastic average volume strain of 0.2%, apparently rises along with increasing wall thickness in Fig. 3(a). More prominent stress concentration occurring on the HPD unit with larger wall thickness can be ascribe to lower strut aspect ratio and larger material (Ni) mass loading, which induce more significant node clamping effect. When the wall thickness increases, the mechanical enhancement of the compressive modulus and strength on the HPD lattice architecture, also can be observed in Fig. 3(b) which is the stress – strain plots for five different PD units. It is found that the rate of mechanical enhancement exceeds the rate of Ni material mass increase as shown in Table 1 with wall thickening. This can be explained in two folds. One reason can still be ascribed to the fact mentioned above, that the lower strut aspect ratio inducing more significant node clamping effect. Another reason is attribute to the bending dominated deformation behavior of the hollow strut. In details, for a given strain ε, a well-defined stiffness is around Et, t is the wall thickness, E is Young's modulus of the constitute material, the tension rigidity and bending rigidity of the hollow strut can be derived as $Et/(1-\nu^2)$ *and* $Et^3/[12(1-\nu^2)]$, respectively, where ν is the Poisson ratio. This qualitatively explains why the compressive modulus of PD lattice architecture increases much faster comparing to the wall thickness increment.

HPD unit cells with wall thickness from 10 μm to 50μm as listed in Table 1 are simulated to derive the relationship between the compressive modulus and relative density of the metallic foam. Note that the FEM simulations for PD unit cell with wall thickness less than 10 μm have not been conducted here. This is due to the extreme thin strut wall in combination with the macroscopic size of the PD structure, which will induce large computation error. In addition, usually with such thin strut wall, the roughness and defects will inevitably reduce the foam mechanical strength, and also

Table 1
Summary of geometry properties of HPD lattices.

Thickness (um)	Volume (10^{-9} m^3)	PD Model Edge Length (mm)	Unit Cell Side Length, L (mm)	Compressive Modulus, E (MPa)	Relative Density, ρ/ρ_s
10	0.196056	1.149520	3.00948278	21.3572	0.007192909
15	0.310754	1.154010	3.02123849	49.9231	0.011268386
20	0.436357	1.158501	3.03299419	80.8553	0.015639657
25	0.572835	1.162991	3.0447499	123.8139	0.020294328
30	0.710157	1.167481	3.0565056	176.2733	0.024870172
35	0.868253	1.171972	3.06826131	244.1481	0.030058635
40	1.037143	1.176462	3.08001701	327.5959	0.035495990
45	1.216795	1.180952	3.09177272	424.7712	0.041171315
50	1.407177	1.185442	3.10352842	542.0802	0.047074048

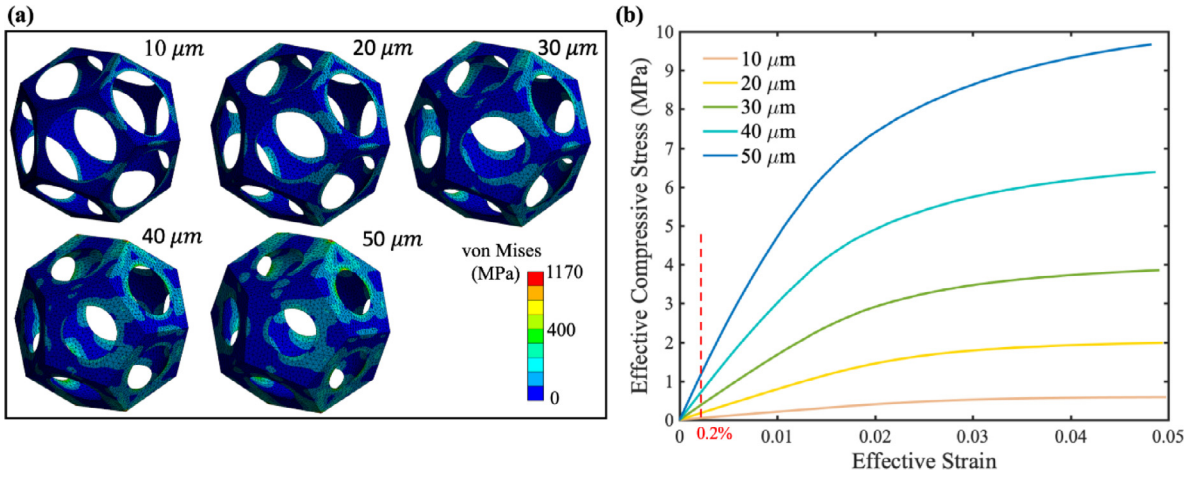

Fig. 3. **(a)** Schematic diagram of the deformation and stress distribution in HPD unit cell with wall thickness ranging from 10 μm to 50 μm,showing the strain localization (stress concentration) and local buckling of the PD truss; (Note: the stress distribution is rendered at 0.2% effective strain.) **(b)** The stress-strain curves of HPD model with Ni as the constituent material. (For interpretation of the references to color in this figure legend, the reader is referred to the web version of this article.)

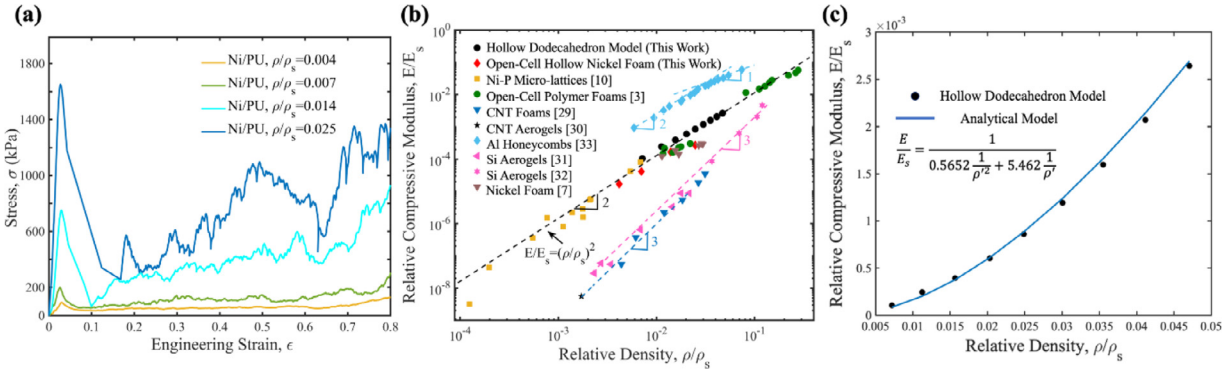

Fig. 4. Modulus and relative density relation: **(a)** Stress-Strain curves of manufactured Ni foams as a function of the coating thickness; **(b)** Relative compressive modulus (defined as the measured Young's modulus, E, divided by the Young's modulus of the constituent solid, E_S) of selected cellular materials at low relative density comparing to HPD model results; **(c)** Quadratic regression fitting for the HPD Model. (For interpretation of the references to color in this figure legend, the reader is referred to the web version of this article.)

lead to a prominent difference for the simulation and experiment results [10].

To validate the as-developed 3D packing HPD lattice architecture for describing mechanical behavior of stochastic metallic foam with hollow struts, the simulation results of effective compressive modulus in Table 1 have been plotted as a function of foam densities and compared to experimental measurements (from both prior studies and this work) in Fig. 4. Fig. 4(a) shows the stress – strain curves of the Ni foam with hollow struts which are manufactured through PU foam templating and electroless-electroplating. The elastic modulus is the maximum slope value obtained by fitting the linear response at small strains found at up to 2.35%, during which the compression and bending of the struts are assumed to dominate the mechanical deformation. The drop of the compressive strength thereafter results from the continuous buckling and failure of struts. [23–26] As observed, both the compressive modulus and strength of the HPD lattice are increasing along with larger wall thickness, which agrees well with the result in Fig. 3. On contrary to thin wall architecture, a distinct stress drops appears in the nickel foam with larger density corresponding to higher wall thickness in Fig. 4(a). To interpret this with our HPD lattice model, as shown in Fig. S1, the maximum stress of the [−1,−1] struts with different wall thickness ranging from 10 to 50 μm are presented. Apparently, the struts with thicker wall bears larger strain localization under same effective engineering strain, which is typically attributed to the surface tension of neighbor circle

and a shorter effective beam length (due to larger nodal volume) resisting the deformation [24]. Moreover, the nanocrystalline (NC) nature of electro-chemical deposited bulk nickel indicates a strong mechanical strength, following the Hall–Petch relation. As small grain size help reducing the strain accumulation. However, under large deformation, dislocations can pile up at the grain boundary eventually resulting a brittle behavior of the NC structure [27,28]. The modulus of the as-manufactured Ni foam is extracted and compared with the simulation results in Fig. 4(b). In contrast, other materials with relative density < 10 mg/cm^3 are plotted, such as CNT foams [29,30], silicon aerogel [31,32] and aluminum honeycombs [33]. As shown, the obtained compressive modulus from the HPD models with wall thickness ranging from 10 μm to 50 μm, performs a nonlinear mechanical property scaling in the factor of two, which is in great agreement with the experimental results. Within the low relative density region ($\rho/\rho_s < 0.01$), a small transition tendency to a different, topology-dependent scaling relation is observed, resulting in an overestimation of the compressive modulus of relative foam. This deviation is ascribed to the neglected defects in HPD model, which exist in the actual metallic foam, such as waviness in the struts [34], non-uniformity of the cross sections [35], misalignment of the nodes, possible defects induced during electroplating procedure, such as small notches, impurities, oxide layer on the strut outer surface and precipitates in the cell wall [23,25,26].

For the HPD lattice architecture, a transition of the foam stiffness scaling from two to one when the struts decrease slenderness of $\lambda \approx 20$ ($\rho/\rho_s \approx 0.1$) to $\lambda \approx 1$ ($\rho/\rho_s \approx 0.01$) is identified, where the slenderness is defined as $\lambda = \sqrt{AL^2/I}$, with A is the cross-section area, and I is the area moment of inertia of the beam. Ignoring the combination effects of bending and stretching in the beam, mechanical properties of lattice architecture normally modeled with either bending or stretching behavior by assuming one dominate the other. To understand this transition and address the complex entanglement of stretching-bending effects as well as the shear deformation, we developed an analytical model based on both Euler and Timoshenko beam theory for accurately capturing the young's modulus of the non-rigid HPD lattice in Fig. S2. Fitting our model with FEM simulation result, the effective young's modulus can be expressed with

$$\frac{E}{E_s} = \frac{1}{0.5652\frac{1}{\rho'^2} + 5.462\frac{1}{\rho'}} \tag{1}$$

Full derivation of this equation is provided in the supplement material. The stiffness transition is similar to the Gibson and Ashby's (GA) bending dominant model [36], which only has a squared term in the fit for modulus of elasticity. Moreover, in a very recent paper, Tereza et al. [37] also numerically calculated the young's modulus of the GA open cell based metamaterial model and claims essentially, for the young's modulus, the perfect three dimensional strut-based metamaterials constructed on open GA cell don't obey the Gibson-Ashby power law prediction, especially in the low relative density region. Beside of that, comparing to experimental results, there are several reasons may affect the stress and strain behavior of the HPD model at low relative density region: (1) in HPD model, the struts are defect free and pristine and thereby bring about the overestimation of the modulus,; (2) as the thickness increases the node becomes larger and stronger, which increases the convergence of strength and stiffness in the lattice at higher density region. Therefore, both simulation artifacts as well as real structure contribute to the overestimation of the HPD model for describing the stiffness of the cellular metallic foam structure in the low density region.

In summary, a new approach to modeling and investigating the mechanical response of hollow Ni foam with periodic 3D packing HPD lattice architecture is proposed. The elastic response results from the numerical simulations on the uniaxial compression of the foam were compared to experiments with good agreement. An in-depth exploration of the mechanical properties using analytical model assuming Timoshenko beam are provided. Our model not only provides an insight explanation of the parameter space of hollow struts-cellular architecture, but also establishes mechanism of the strength and the stiffness governed by the intricate entanglement of geometry and structure. Moreover, it provides a simple way to accurately predict the mechanical properties of open-cell cellular foam structure. During our discussion, we postulate that the convergence of strength and stiffness in the lattice at high density is caused by the increased influence of the beam intersections at the node. As the thickness increasing, the node becomes larger and stronger. However, the strength and stiffness parameter space of hollow lattices is highly complex and depends not only on the beam length, radius and thickness but also on the space topology organization for the full-scale foam. Overall, this work provides a new prospect to estimate the mechanical properties of the stochastic cellular structure.

Declaration of Competing Interest

The authors declare that they have no known competing financial interests or personal relationships that could have appeared to influence the work reported in this paper.

Acknowledgment

This study is partially supported by ASU startup funds, NSF grants CMMI-1825576 and CMMI-1826439. We acknowledge the use of facilities within the Eyring Materials Center at Arizona State University supported in part by NNCI-ECCS-1542160. The Instron E3000 was obtained using funds from the Army Research Office (W911NF-15-1-0353).

Supplementary materials

Supplementary material associated with this article can be found, in the online version, at doi:10.1016/j.scriptamat.2020.03.001.

References

[1] J. Paulose, A.S. Meeussen, V. Vitelli, Proc. Natl. Acad. Sci. 112 (25) (2015) 7639–7644.
[2] J. Banhart, Prog. Mater. Sci. 46 (6) (2001) 559–632.
[3] Q. Wang, J.A. Jackson, Q. Ge, J.B. Hopkins, C.M. Spadaccini, N.X. Fang, Phys. Rev. Lett. 117 (17) (2016) 175901.
[4] A. Buhrig-Polaczek, T. Guillen, A. Ohrndorf, H.J. Christ, K. Hagemann, U. Krupp, Removal of the α-Case Layer from Precision-Cast Cellular TiAl6Nb7 to be Used for Biomedical Applications, Adv. Eng. Mater. 11 (8) (1982) 680–684.
[5] G.J. Davies, S. Zhen, J. Mater. Sci. 18 (7) (1983) 1899–1911.
[6] H.N.G. Wadley, Adv. Eng. Mater. 4 (10) (2002) 726–733.
[7] M.M. Shbeh, R. Goodall, Met. Powder Rep. 71 (6) (2016) 450–455.
[8] D.T. Queheillalt, D.D. Hass, D.J. Sypeck, H.N.G. Wadley, J. Mater. Res. 16 (4) (2001) 1028–1036.
[9] M.G. Rashed, M. Ashraf, R.A.W. Mines, P.J. Hazell, Mater. Des 95 (2016) 518–533.
[10] A. Torrents, T.A. Schaedler, A.J. Jacobsen, W.B. Carter, L. Valdevit, Acta Mater. 60 (8) (2012) 3511–3523.
[11] T.A. Schaedler, A.J. Jacobsen, A. Torrents, A.E. Sorensen, J. Lian, J.R. Greer, L. Valdevit, W.B. Carter, Science 334 (6058) (2011) 962–965.
[12] J.H. Martin, D.S. Ashby, T.A. Schaedler, Mater. Des. 120 (2017) 291–297.
[13] D.T. Queheillalt, Y. Katsumura, H.N.G. Wadley, Scr. Mater. 50 (3) (2004) 313–317.
[14] A. Jung, S. Diebels, Adv. Eng. Mater. 18 (4) (2016) 532–541.
[15] W.E. Warren, A.M. Kraynik, J. Appl. Mech. 64 (4) (1997) 787–794.
[16] K. Boomsma, D. Poulikakos, Y. Ventikos, Int. J. Heat Fluid Flow 24 (6) (2003) 825–834.
[17] Y.W. Kwon, R.E. Cooke, C. Park, Mater. Sci. Eng. A 343 (1–2) (2003) 63–70.
[18] C. Petit, S. Meille, E. Maire, J. Mater. Res. 28 (17) (2013) 2191–2201.

[19] D.L. Duan, R.L. Zhang, X.J. Ding, S. Li, Mater. Sci. Technol. 22 (11) (2006) 1364–1367.
[20] T. Fiedler, E. Solórzano, F. Garcia-Moreno, A. Öchsner, I.V. Belova, G.E. Murch, Adv. Eng. Mater. 11 (10) (2009) 843–847.
[21] A. Zenner, D. Edouard, Appl. Therm. Eng. 113 (2017) 1313–1318.
[22] X.W. Gu, J.R. Greer, Extreme Mech. Lett. 2 (2015) 7–14.
[23] E. Amsterdam, P.R. Onck, J.T.M. De Hosson, J. Mater. Sci. 40 (22) (2005) 5813–5819 0022-2461.
[24] E. Amsterdam, J.H.B. De Vries, J.T.M. De Hosson, P.R. Onck, Acta Mater. 56 (3) (2008) 609–618 1359-6454.
[25] P.R. Onck, R. Van Merkerk, A. Raaijmakers, J.T.M. De Hosson, J. Mater. Sci. 40 (22) (2005) 5821–5828 0022-2461.
[26] P.R. Onck, R. Van Merkerk, J.T.M. De Hosson, I. Schmidt, Adv. Eng. Mater. 6 (6) (2004) 429–431 1438-1656.
[27] J.B. Jeon, B.-J. Lee, Y.W. Chang, Scr. Mater. 64 (6) (2011) 494–497 1359-6462.
[28] J. Li, B. Lu, H. Zhou, C. Tian, Y. Xian, G. Hu, R. Xia, Phys. Lett. A 383 (16) (2019) 1922–1928 0375-9601.
[29] M.A. Worsley, S.O. Kucheyev, J.H. Satcher Jr, A.V. Hamza, T.F. Baumann, Appl. Phys. Lett. 94 (7) (2009) 073115 0003-6951.
[30] J. Zou, J. Liu, A.S. Karakoti, A. Kumar, D. Joung, Q. Li, S.I. Khondaker, S. Seal, L. Zhai, ACS Nano 4 (12) (2010) 7293–7302 1936-0851.
[31] M. Moner-Girona, A. Roig, E. Molins, E. Martınez, J. Esteve, Appl. Phys. Lett. 75 (5) (1999) 653–655 0003-6951.
[32] T.M. Tillotson, L.W. Hrubesh, J. Non-Cryst. Solids 145 (1992) 44–50 0022-3093.
[33] H.H. Attributes, the technical document issued by the Hexcel composites company, available on the www.hexcel.com internet site (38 pages) (1999) 3.
[34] D. Queheillalt, V. Deshpande, H. Wadley, J. Mech. Mater. Struct. 2 (9) (2007) 1657–1675 1559-3959.
[35] M.A. Fortes, M.F. Ashby, Acta Mater. 47 (12) (1999) 3469–3473 1359-6454.
[36] L.J. Gibson, Proc. R. Soc. Lond. A 382 (1782) (1982) 43–59.
[37] T. Uhlířová, W. Pabst, Scr. Mater. 159 (2019) 1–4.